Voltage-current Characteristics of MHD Boundary Layer Plasmas

AUTHOR(S):

HARA, Takehisa; HAYASHI, Muneaki

CITATION:

HARA, Takehisa ...[et al]. Voltage-current Characteristics of MHD Boundary Layer Plasmas. Memoirs of the Faculty of Engineering, Kyoto University 1987, 49(4): 280-293

ISSUE DATE:

1987-11-30

URL:

http://hdl.handle.net/2433/281360

Voltage-current Characteristics of MHD Boundary Layer Plasmas

By

Takehisa HARA and Muneaki HAYASHI

(Received June 26, 1987)

Abstract

This paper deals with a two-dimensional time-dependent numerical simulation of the growth of discharges in MHD generator boundary layers. The calculated voltage-current characteristics in a boundary layer have positive resistance characteristics for small currents and negative ones for large currents. The characteristics agree with those observed in an anodic layer of actual ETL-Mark 7 B-channel experiments for various temperatures of electrodes. The current flows almost uniformly into the electrode surface (diffuse or fine constricted mode) when the current density is in the region of positive *V-I* characteristics. It concentrates in a large diameter (large constricted mode) in the region of negative ones. The critical current for this transition of discharge mode is about 0.5 A/cm^2 for cold electrodes. This value becomes larger for hot electrodes.

1. Introduction

The decrease of electrode lifetime caused by erosion due to local current concentration is one of the serious problems of an open-cycle MHD power generator[1]. Therefore, it is normally desired that MHD plasmas conduct current in a diffuse mode, i.e., that the current be locally distributed throughout the plasma and not form concentrations, or other arc-like structures. The constricted mode is characterized by patterns of locally intense levels of Joule heating in a discharge. The bulk of the current flow is confined to these locally isolated regions of the overall conduction domain.

Although a variety of constricted effects are possible in an MHD plasma, a constricted discharge is commonly observed to occur near the electrode walls. Because of the requirement of current continuity from gas to metal, a constricted or arc spot regime is often required to provide local heating and emission from the conductor. This metal-gas arc spot region is confined to a very thin layer of the order of Debye lengths near the conductor surface. In addition to this peculiarly gas-metal transition region, there also exists a purely gas-phase constriction which

is possible and develops when a high current density is forced through a cool electrode wall gas dynamic boundary layer. The principal features of this inherently gas-phase constriction may be understood in terms of a simple requirement of minimum impedance of the current path in the presence of a low conductivity layer. It is principally this gas-phase constriction to which the present study is directed.

There have been many studies about constricted or arc discharges in MHD generator boundary layers.[2-7] Oliver[4] discussed the generation of current constriction in the plasma near the electrode by considering the energy balance for quantities perturbed from the diffuse mode. Okazaki[6] did more detailed study along this line. While the objective of much of this past theoretical work has been to determine the stability limit, Rosa[7] examined the characteristics of the arc after initiation.

The present study deals with a two-dimensional time-dependent numerical simulation of the growth of constricted discharges in MHD generator boundary layers. By simulation, not only the process of transition from a diffuse discharge mode to a constricted one, but also the characteristics of the constricted discharge after it is formed can be made clear.

2. Theoretical Model

Basic Equation

The mathematical model for calculating the current and potential distributions in open cycle MHD channels is given by the following Maxwell's equations:

$$\nabla \times \boldsymbol{E} = 0 \tag{1}$$

$$\nabla \cdot \boldsymbol{j} = 0 \tag{2}$$

together with a generalized Ohm's law written as

$$\boldsymbol{j} = \sigma(\boldsymbol{E}+\boldsymbol{u}\times\boldsymbol{B}) - (\beta/B)\,(\boldsymbol{j}\times\boldsymbol{B}) \tag{3}$$

where $\boldsymbol{j}$ is the current density, $\boldsymbol{E}$ the electric field, $\boldsymbol{u}$ the gas velocity, $\boldsymbol{B}$ the applied magnetic field, and σ and β are the electrical conductivity of the gas and Hall parameter, respectively.

For the combustion gas used in the calculation, the electrical conductivity and Hall parameter are given by the following equations:

$$\sigma = 89.9\, p^{-0.51}\, T^{1.055} \exp(-2.52\ 10^4/T) \quad S/m \tag{4}$$

$$\beta = 4.43\ 10^{-4}\, p^{-0.99}\, T^{0.97} \quad B \tag{5}$$

where T is the gas temperature and p the static pressure.

The temperature of the gas is governed by the following energy balance equation:

$$\rho C_p(\partial T/\partial t) = \nabla\cdot(\kappa\nabla T)+j^2/\sigma+\boldsymbol{u}\cdot(\boldsymbol{j}\times\boldsymbol{B}) \tag{6}$$

where ρ is the total mass density, C_p the specific heat at constant pressure and κ the thermal conductivity. The losses due to convection and radiation are neglected in Eq. (6). In the boundary layers, a sharp temperature gradient will be produced by the local joule heating.

Two-dimensional Model

All quantities are assumed to be constant in the direction of the magnetic field and the calculations are made in the plane perpendicular to the direction. The coordinate system and channel geometry used in the calculations are shown in Fig. 1. The gas velocity and the magnetic field are assumed to have the form $\boldsymbol{u}=(u, 0, 0)$ and $\boldsymbol{B}=(0, 0, B)$ in which u is constant in time and B is constant in space and time.

Using the above assumptions, Eqs. (1)–(3) are reduced to the following set:

$$\partial E_y/\partial x-\partial E_x/\partial y = 0 \tag{7}$$

$$\partial j_x/\partial x+\partial j_y/\partial y = 0 \tag{8}$$

$$E_x = (j_x+\beta j_y)/\sigma\,,\quad E_y = (-\beta j_x+j_y)/\sigma+uB \tag{9}$$

Current Stream Function

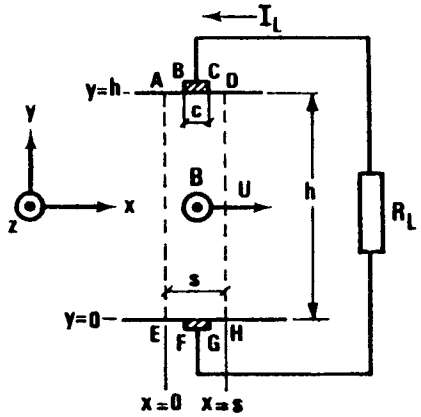

Fig. 1. Coordinate system and channel geometry.

Eq. (8) permits the representation of $\boldsymbol{j}$ in terms of a current stream function ψ defined by

$$j_x = (I_L/w)\ (\partial\psi/\partial y)\ , \quad j_y = -(I_L/w)\ (\partial\psi/\partial x) \tag{10}$$

where I_L is the load current and w the channel width. An equation for ψ is developed by substituting Eqs. (9) and (10) into Eq. (7) as

$$\partial[(1/\sigma)\ (\partial\psi/\partial x)+(\beta/\sigma)\ (\partial\psi/\partial y)]/\partial x$$
$$-\partial[(\beta/\sigma)\ (\partial\psi/\partial x)-(1/\sigma)\ (\partial\psi/\partial y)]/\partial y = 0 \tag{11}$$

In order to solve Eq. (11), the boundary conditions have to be specified over the perimeter of the calculation plane. For a channel with electrodes and insulators arranged in an infinitely long periodic structure, the periodicity can be assumed over one segment. Therefore, the calculations are made in one segment region (AEHD) in Fig. 1. The boundary condition on the electrode is $E_x=0$ and by using Eqs. (9), (10) it becomes

$$\beta\partial\psi/\partial x-\partial\psi/\partial y = 0 \quad \text{(on BC and FG)} \tag{12}$$

On the insulators, $j_y=0$ is given and substitution of Eq. (10) yields $\psi=$const. on AB, CD, EF and GH. By definition, ψ is taken equal to zero on the left insulator, namely

$$\psi = 0 \quad \text{(on AB and EF)} \tag{13}$$

The integration of j_y over the electrode gives the load current I_L,

$$I_L = -w\int_B^C j_y\, dx \tag{14}$$

Substituting Eq. (10) into Eq. (14) yields

$$I_L = w\int_B^C (I_L/w)\ (\partial\psi/\partial x)\ dx = I_L[\psi(C)-\psi(B)]$$

Finally, we obtain

$$\psi(C)-\psi(B) = 1 \tag{15}$$

By considering Eqs. (13) and (15), ψ must be unity on the right insulator, namely

$$\psi = 1 \quad \text{(on CD and GH)} \tag{16}$$

Since periodicity is assumed over the one segment, the boundary condition on DH

and AE is given as,

$$\psi \text{ (on DH)} - \psi \text{ (on AE)} = 1 \tag{17}$$

Load Current

Having found the value of ψ, j_x and j_y are obtained from Eq. (10). However, in order to do this, the value of I_L should be known. By integrating Eq. (9) over the line $x=s/2$, we obtain

$$\int_0^h (E_y|_{x=1/2s} - uB)\, dy = \int_0^h (-j_x+j_y)/\sigma|_{x=1/2s}\, dy \tag{18}$$

Since each electrode is connected to an external load R_L, as shown in Fig. 1, the next relation should be satisfied,

$$\int_0^h E_y|_{x=1/2s}\, dy = R_L I_L \tag{19}$$

Substituting this relation and Eq. (10) into Eq. (18) yields,

$$R_L I_L - uBh = -(I_L/w)\int_0^h (\beta\partial\psi/\partial y + \partial\psi/\partial x)/\sigma|_{x=1/2s}\, dy$$

Finally,

$$I_L = uBh/[R_L + (1/w)\int_0^h (\beta\partial\psi/\partial y + \partial\psi/\partial x)/\sigma|_{x=1/2s}\, dy] \tag{20}$$

Here it is obvious that the second term of the denominator of the right-hand side of Eq. (20) corresponds to the internal resistance of the plasma. After calculating the value of I_L from this equation, we can obtain j_x and j_y from Eq. (10).

Gas Temperature

By the two-dimensional assumption, the energy balance equation (6) is reduced to

$$\rho C_p(\partial T/\partial t) = \partial(\kappa\cdot\partial T/\partial x)/\partial x + \partial(\kappa\cdot\partial T/\partial y)/\partial y + (j_x^2+j_y^2)/\sigma + uj_yB \tag{21}$$

The boundary conditions for gas temperature T are given by

$$T = Tw \quad \text{(on AD and EH)} \tag{22}$$

$$T\text{ (on AE)} = T\text{ (on DH)} \tag{23}$$

where Tw is the electrode wall temperature. In the core region, the gas temper-

ature is assumed to have the constant value T_∞, which means that the gas temperature in the boundary layer region changes according to Eq. (21). The initial gas temperature distribution is assumed to belong to the (1/7) th power law.

3. Numerical Simulations of the Discharges in MHD Boundary Layers

Numerical Procedure

The partial differential Equations (11) and (21) for ψ and T respectively, are solved iteratively by using the finite element method. Bilinear rectangular elements are employed in the calculation. One pitch region is divided into 36 (x direction) $\times 30$ (y direction) $=1440$ elements. The even meshes are employed in x direction and the uneven meshes in y direction. The time step Δt is selected as 25 μs so as to satisfy the stability condition.

Geometrical and Gasdynamic Conditions

In order to compare the numerical results with the experimental ones, the dimensions of the channel used in the calculations have been chosen equal to that of the ETL-Mark 7 B-channel, i.e., channel height $h=24$ cm, channel width $w=7.5$ cm, one pitch length $s=2.4$ cm, and electrode width $c=2.0$ cm. The gasdynamic conditions are also chosen to have almost the same values as the experimental ones, i.e., gas core temperature $T=2500$ K, static pressure $p=2$ atm, magnetic field $B=2.5$ T, thermal conductivity $\kappa=1.5$ J/(msK), boundary layer width $\delta=3.0$ cm.

Growth of Constricted Discharges

The two-dimensional time dependent behaviors of the discharges in the channel, especially in the boundary layers, are numerically simulated under the geometrical and gasdynamic conditions mentioned above. For $t>0$, the channel is assumed to be open circuited and the electrodes are connected to the external loads at $t=0$. The development of the current constriction for the case of the electrode wall temperature $Tw=400$ K is illustrated at eight time instances ($t=0$, 20, 40, 60, 80, 100, 300×25 μs) in Fig. 2. Though the calculation is done in one pitch regior, three pitch regions are shown in the figure. The current constriction occurs at $t=1.5$ ms (60×25 μs) and it grows with time. It reaches an almost steady state at about $t=7.5$ ms (300×25 μs), and the current density or the current distribution scarcely changes after that.

Potential Distributions between the Anode and the Cathode

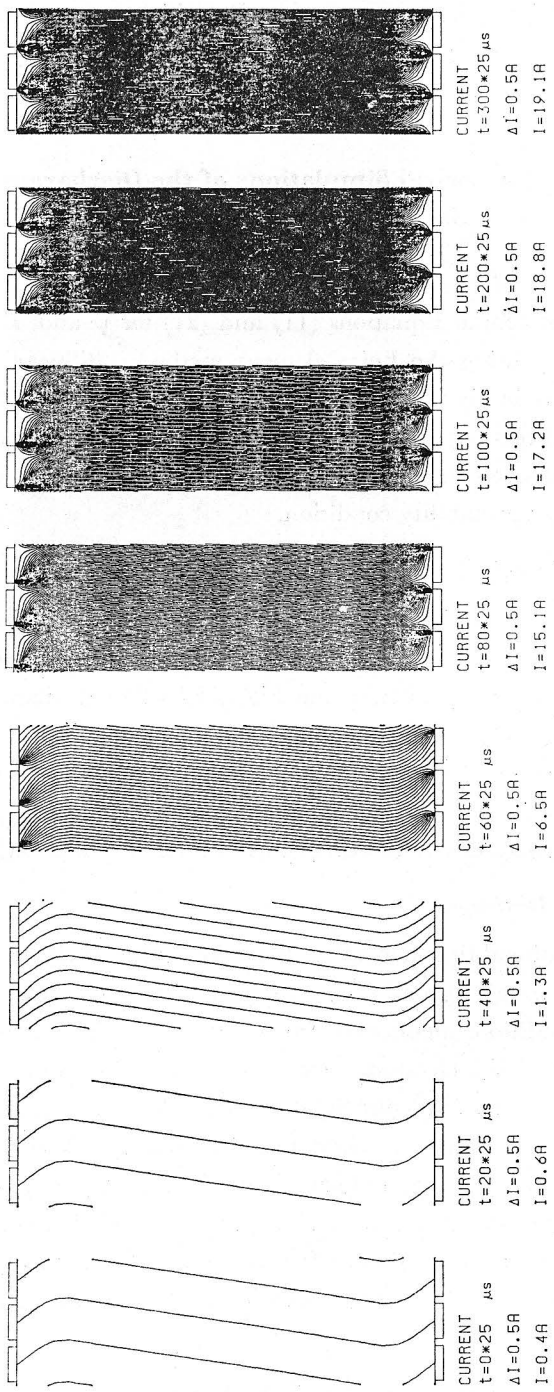

Fig. 2. Time history of the current streamline distributions in the channel.

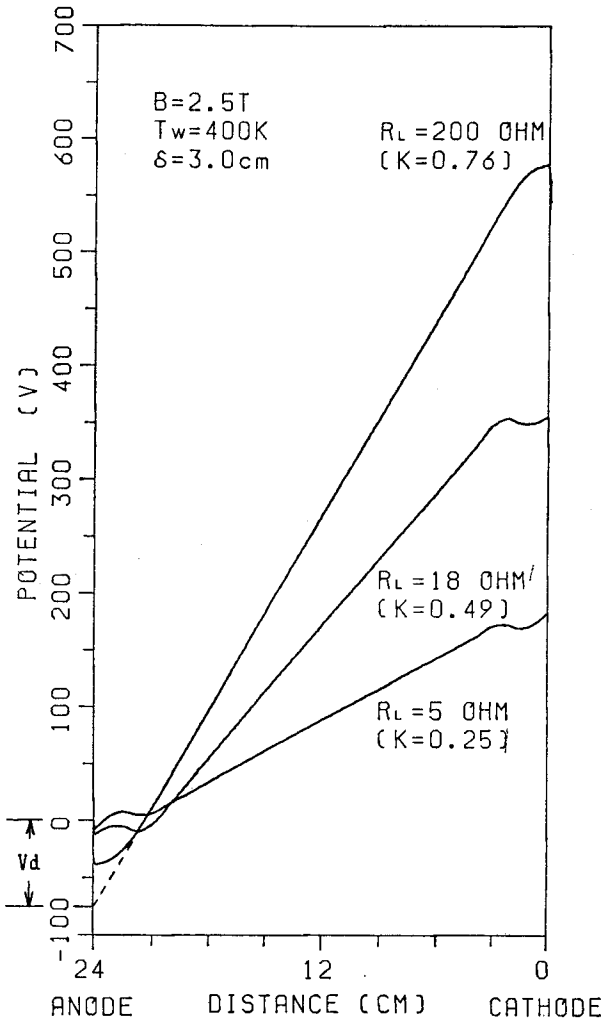

Fig. 3. The potential distribution between the anode and the cathode.

In this section, we will focus on the behavior of the discharge after it arrives at a final current and potential distribution. The calculated potential distributions between the anode and the cathode for load resistance R_L=5, 18 and 200 Ω are shown in Fig. 3. Since the electrode surface phenomena are neglected in the calculation, the potential distributions are the same on both the anode and the cathode. The electrode voltage drop V_d is obtained as shown in the figure.

4. Voltage-Current Characteristics of Boundary Layer Plasmas

V-I Characteristics for Different Electrode Wall Temperature

From the potential distributions along the boundary layer, it is possible to

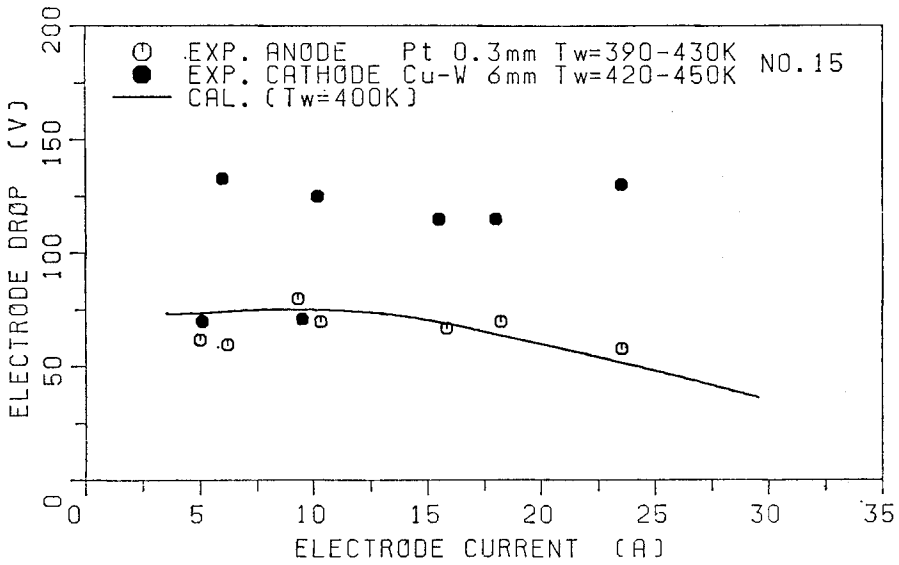

(a) Tw=400 K

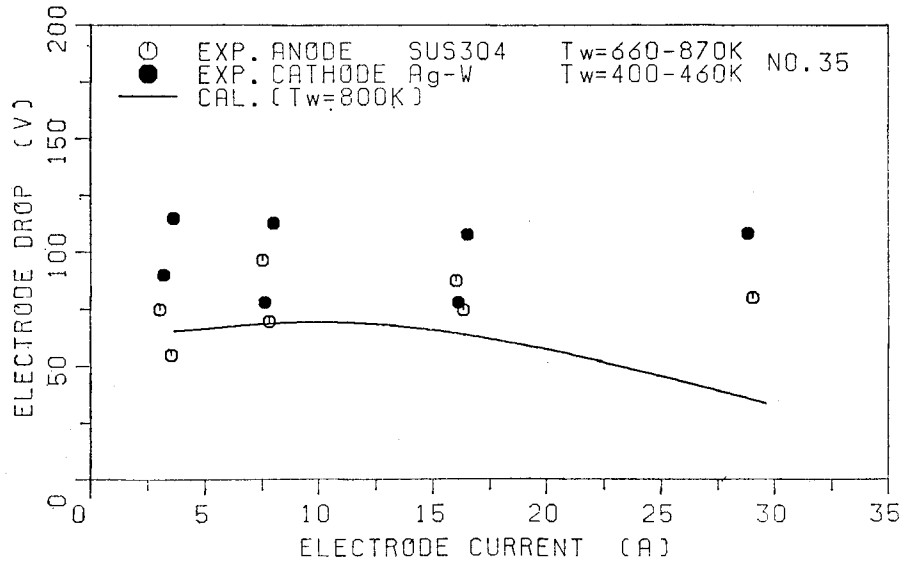

(b) Tw=800 K

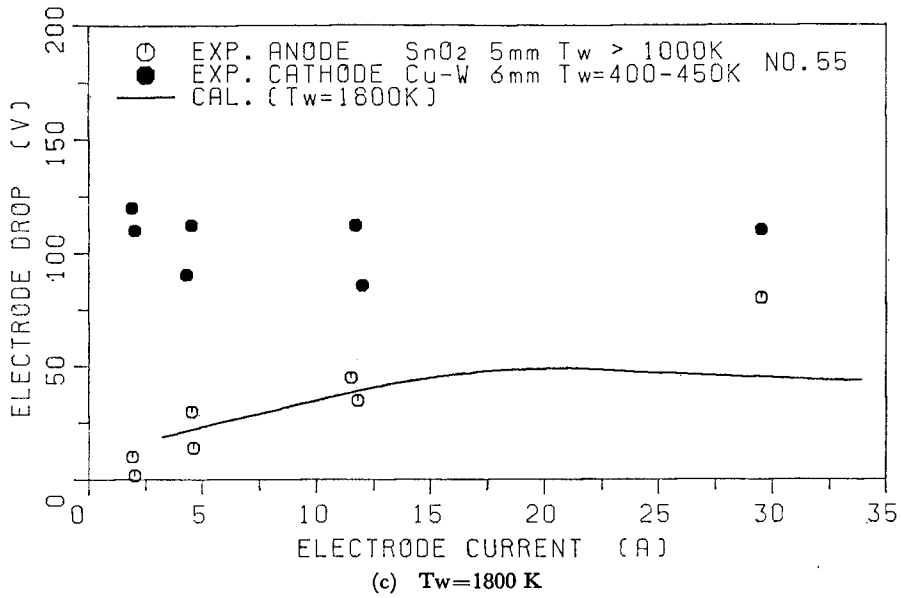

(c) Tw=1800 K

Fig. 4. Variations of electrode voltage drops with load current.

calculate the electrode voltage drop. The variations of the electrode voltage drop with current for three different electrode wall temperatures, Tw=400, 800, and 1800 K, are shown in Fig. 4 (a), (b), and (c), respectively. The experimental values of the voltage drop on the anode and cathode in the ETL-Mark 7 B-channel are also plotted in the figures. It is found from these three figures that the calculated *V-I* characteristics agree well with those observed on the anode experiments. Because the electrode surface phenomena such as the thermionic emission from the electrode is neglected in the calculation, it is quite natural that the calculated results do not agree with the experimental ones of the cathode from which the thermionic emission is thought to be active.

It is found from both the experimental and calculated results that the *V-I* characteristics are composed of two parts, namely a positive resistance characteristic part and a negative one. The positive part corresponds to the small current region and the negative part to the large one.

Discharge Mode for Small and Large Currents

In this section, let us investigate the discharge modes of currents corresponding to the positive and negative *V-I* characteristics. The calculated final current streamline, gas temperature, current density and electrical conductivity distributions in the boundary layer for the electrode wall temperature Tw=400 K are shown in

Fig. 5, Fig. 6, Fig. 7 and Fig. 8, respectively. Two sets of those distributions corresponding to (a) positive and (b) negative *V-I* characteristics are shown in each figure. For the electrode wall temperature Tw=400 K, it is seen from these figures that the current concentrates for both positive and negative cases, but their sizes are quite different. When the current is in the range of positive *V-I* characteristics, the current concentration is very small (fine constricted mode), and when it is in the range of negative ones, it concentrates in a large diameter (large constricted mode). The gas temperature of the concentrated part of the fine constricted more is 2500 K, the current density is 2 A/cm^2 and the electrical conductivity is 10 S/m. In the concentrated part of the large constricted mode the gas temperature is 3500 K, the current density 20 A/cm^2 and the electrical conductivity 800 S/m.

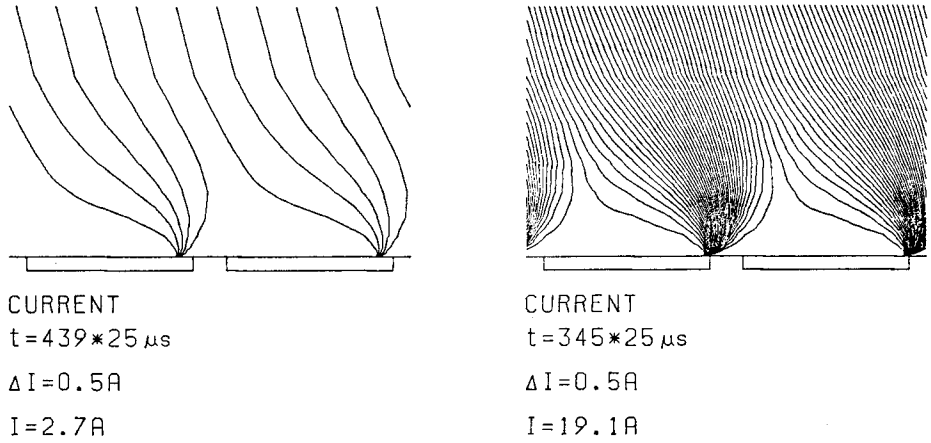

(a) Positive V-I characteristics (b) Negative V-I characteristics

Fig. 5. Current streamline distributions in the boundary layer for Tw=400 K.

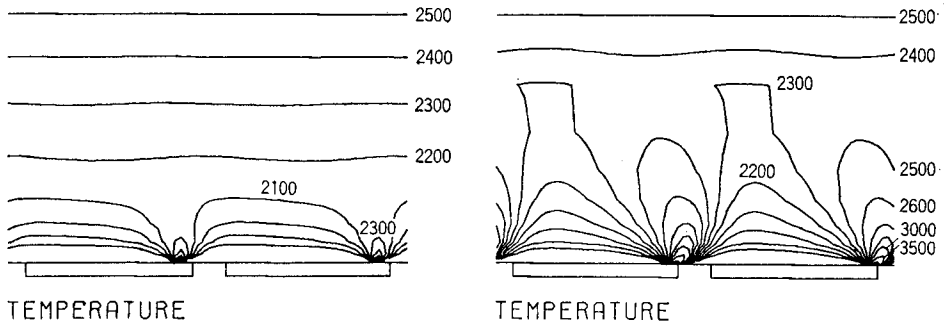

(a) Positive V-I characteristics (b) Negative V-I characteristics

Fig. 6. Gas temperature (K) distributions in the boundary layer forTw=400 K.

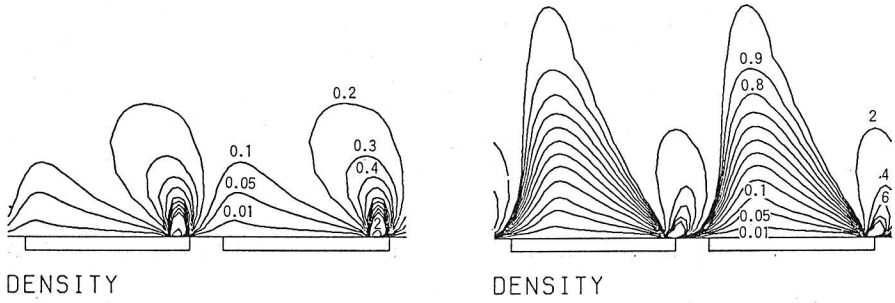

(a) Positive V-I characteristics (b) Negative V-I characteristics

Fig. 7. Current density (A/cm²) distributions in the boundary layer for Tw=400 K.

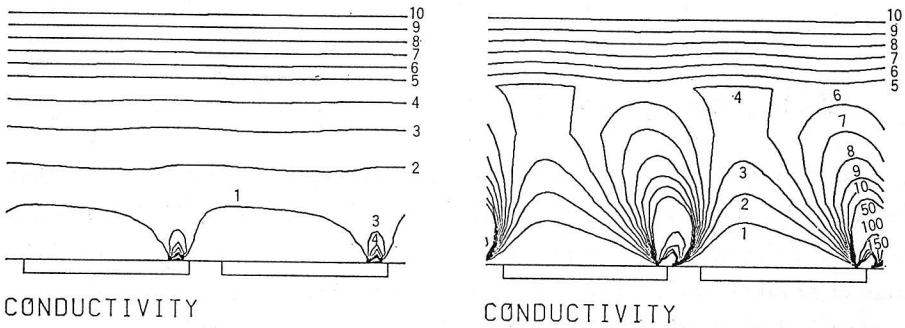

(a) Positive V-I characteristics (b) Negative V-I characteristics

Fig. 8. Electrical conductivity (S/m) distributions in the boundary layer for Tw=400 K.

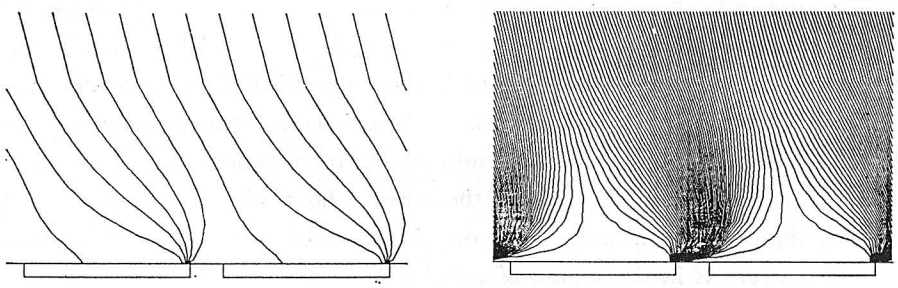

(a) Positive V-I characteristics (b) Negative V-I characteristics

Fig. 9. Current streamline distributions in the boundary layer for Tw=800 K.

Fig. 9 and Fig. 10 show the current streamline distributions in the boundary layer for the electrode wall temperatures *Tw*=800 and 1800 K, respectively. In

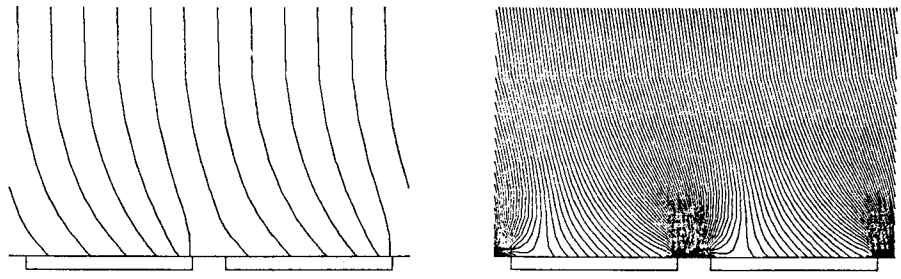

(a) Positive V-I characteristics (b) Negative V-I characteristics

Fig. 10. Current streamline distributions in the boundary layer for Tw=1800 K.

the case of the electrode wall temperature Tw=800 K, it is seen from Fig. 9 that the discharge also shows a fine constricted mode when the current is in the range of positive *V-I* characteristics, and a large constricted mode when the current is in the range of negative ones. The calculated gas temperature, the current density and the electrical conductivity of the concentrated part are almost the same as the case of Tw=400 K for both fine and large constricted modes.

The current in the range of positive *V-I* characteristics flows almost uniformly onto the electrode surface (Fig. 10 (a)) at Tw=1800 K, which we call a diffuse discharge mode. However, the current in the range of negative ones concentrates in a large diameter (Fig. 10 (b)) in which the gas temperature is calculated to be 3000 K, the current density 20 A/cm^2 and the electrical conductivity 400 S/m.

Summarizing the above results, the current flows almost uniformly (diffuse mode) or slightly concentrated (fine constricted mode) onto the electrode surface when the current is in the region of positive *V-I* characteristics. It concentrates in a large diameter (large constricted mode) in the region of negative ones. The critical current density for this transition of the discharge mode is about 0.5 A/cm^2 for cold electrodes. This value becomes larger for hot electrodes.

5. Conclusions

This paper deals with a two-dimensional, time-dependent numerical simulation of the growth of constricted discharges in a MHD channel, especially in the boundary layers. The following conclusions are derived from the calculations:

(1) The voltage-current characteristics in a MHD boundary layer have positive resistance characteristics for small currents and negative ones for large currents.
(2) The characteristics agree with those observed in an anodic layer of actual ETL-Mark 7 B-channel experiments for various temperatures of electrodes.
(3) The current flows almost uniformly onto the electrode surface (diffuse or fine constricted mode) when the current density is in the region of positive *V-I* characteristics. It concentrates in a large diameter (large constricted mode) in the region of negative ones.
(4) For the case of the electrode wall temperature $Tw=400$ K, the gas temperature of the concentrated part of the fine constricted mode is 2500 K, the current density is 2 A/cm^2 and the electrical conductivity is 10 S/m.
(5) In the concentrated part of the large constricted mode for $Tw=400$ K, the gas temperature is 3500 K, the current density 20 A/cm^2 and the electrical conductivity 800 S/m.
(6) The critical current for the transition of the discharge modes is about 0.5 A/cm^2 for cold electrodes, and it becomes larger up to 1 A/cm^2 for hot electrodes.

Acknowledgements

The authors would like to express their thanks to Mr. Ryogo Yanagisawa and Mr. Shuichi Obayashi of Kyoto university for their computing works. Also, the authors would like to acknowledge the financial support provided by the Grant-in-Aid for Scientific Research from the Ministry of Education, Science and Culture of Japan.

References

1) Kusaka, Y., Takano, K. et al., "Experimental Investigation on ETL Mark VII MHD Facility," 21th Symposium on Engineering Aspects of MHD, Argonne, Illinois, 1983, pp. 2.8.1–16.
2) Messerle, H. K., Sakuntala, M. and Trung, D., "Arc Transition in MHD Generator," J. Phys. D, Vol. 3, 1970, pp. 1080–1088.
3) Hsu, M. S. S., "Thermal instabilities and Arcs in the MHD Boundary Layers," 13th Symposium on the Engineering Aspects of MHD, Stanford, CA., 1973, pp. VI.6.1–6.
4) Oliver, D. A., "A Constricted Discharge in Magnetohydrodynamic Plasma," 15th Symposium on Engineering Aspects of MHD, Philadelphia, PA., 1976, pp. IX.4.1–4.
5) Kon, T., Kayukawa, N., Ozawa, Y. and Aoki, Y., "Electrical and Thermal Instabilities in the Electrodes Surface Region in a Combustion MHD Generator Channel," 16th Symposium on Engineering Aspects of MHD, Pittsburgh, PA., 1977, pp. VI.1.1–4.
6) Okazaki, K., Mori, Y. Hijikata, K. and Ohtake, K., "MHD, Boundary Layer of the Seeded Combustion Gas Near Cold Electrodes," AIAA Journal, Vol. 18, No. 1, 1980, pp. 39–46.
7) Rosa, R. J., "Boundary Layer Arc Behavior," 8th International Conference on MHD Electrical Power Generation, Moscow, 1983, pp. D.6.1–9.